Energy 251 (2022) 123873

Contents lists available at ScienceDirect

Energy

journal homepage: www.elsevier.com/locate/energy

A methodology for techno-economic and operation strategy optimisation of micro gas turbine-based solar powered dish-engine systems

Mohsen Ghavami*, Jafar Al-Zaili, Abdulnaser I. Sayma

Department of Mechanical Engineering and Aeronautics, City, University of London, Northampton Square, London, EC1V 0HB, UK

ARTICLE INFO

Article history:
Received 27 June 2021
Received in revised form
8 March 2022
Accepted 29 March 2022
Available online 5 April 2022

ABSTRACT

This paper focuses on the optimisation of small-scale micro gas turbines totally powered by the concentrated solar power to generate electricity in the range of 5–30kWe. The objective of this paper is to investigate of the potential of such systems for solar power generation at reasonable costs. The computational model uses a component-based approach for thermodynamic performance simulation and features an integrated economic model which allows for the evaluation of economic performance indicators including levelised cost of electricity. The integrated model is coupled to a genetic algorithm optimisation framework to find system designs with optimal techno-economic performance. Two cases of fixed 5kWe rated power and 5-30kWe systems are studied. The performance simulation considers the operation strategy and the safe operation limits. A multi-objective optimisation is performed for each case to find trade-offs between the performance and cost of the system. The levelised cost of electricity and annual solar to electric efficiency are considered for comparison purposes. Results show that a levelised cost of electricity of about 170€/MWh can be achieved for a system installed in Italy. Lower cost of electricity as low as 85€/MWh could be achieved when considering economy of scale and locations with higher annual insolation.

1. Introduction

Concerns about the environmental impact of burning fossil fuels have motivated extensive research and development of renewable energy systems, among the most promising of which is solar power. The European Commission has recommended a perspective of increasing the solar electricity production to 12 TWh per year by 2030 and to 42 TWh per year by 2050 [1]. Photovoltaic (PV) panels are currently well established in the market and their prices have been reducing over the past years. However, concentrated solar thermal (CST) systems coupled with efficient thermodynamic engines are expected to contribute a major part of the solar power sector in the future because of their higher efficiency and power density compared to PV panels [2]. Additionally, such systems offer the potential for reasonable power dispatchability due to the practicality of integration with thermal energy storage as investigated by several work including the InnovateUK funded SolGATS project [3]. There are also rising environmental concerns with the production of PV panels not only because they involve the use of minerals with limited sources on earth [4], but also because the hazardous materials and heavy metals emissions including Nickel, Mercury, Arsenic and Lead occur in those production processes [5,6].

A significant volume of the research undertaken on CST systems focused on the utilisation of the gas turbine engines. Solar powered gas turbine systems can be divided into two main categories: pure solar (also called solar-only) systems, where the sun is the sole provider of the thermal input to the system, and hybrid solar systems which use auxiliary combustion to compensate for the variations of solar irradiation. Most of the research projects have used hybrid arrangements using gas turbines and smaller scale micro gas turbine (MGT) technology. This includes the European Commission funded projects, SOLGATE [7] at rated power of 240kWe, SOLHYCO [8] which used Turbec100 and SOLUGAS which scaled up the developed technology to few MW power range [9]. Despite the progress made in hybrid solar systems, they have some technical difficulties such as the flame instability when a low fuel flow is injected into the combustor as discussed by Refs. [10,11]. Solar-only

* Corresponding author.
E-mail address: m.ghavami@city.ac.uk (M. Ghavami).

https://doi.org/10.1016/j.energy.2022.123873

Nomenclature

Greek letters

α	Capital recovery factor
$\alpha_{rec\upsilon}$	Absorptivity of the receiver
β	Auxiliary coordinate, compressor map
γ	Heat capacity ratio
δ_w	Recuperator wall thickness (m)
Δp	Pressure drop (Pa)
ε	Recuperator effectiveness
$\varepsilon_{rec\upsilon}$	Emissivity of the receiver
σ	System Design point indicator
η	Efficiency
η_{opt}	Optical-to-thermal efficiency
μ	Viscosity (Ns/m^2)
π	Pressure ratio
ρ	Density (kg/m^3)

Variables

a, b, c	Multiplier parameters in cost function
C_{aux}	Cost of auxiliary systems (€1000)
C_{com}	Cost of commissioning (€1000)
C_{inst}	Cost of installation (€1000)
$C_{in\upsilon}$	Cost of investment (€1000)
C_{maint}	Cost of maintenance (€1000)
C_{max}	Maximum heat capacity rate (W/K)
$C_{MGT,m}$	Cost of MGT package (€1000)
C_{min}	Minimum heat capacity rate (W/K)
C_{op}	Cost of operation (€1000)
$c_{MGT,m}$	Specific cost of MGT (€1000/kg s^{-1})
c_p	Specific heat at constant pressure (J/kgK)
C_r	Ratio of the heat capacity rates
CR_g	Geometrical concentration ratio
D_h	Hydraulic diameter (m)
E_{an}	Annual generated electricity (MWh)
G	Volumetric flow rate (kg/m^{2}s)
h	Enthalpy (J/kg) and heat transfer coefficient (W/m^{2}K)
i	Real interest rate
I	Electric current (A)
J	Colburn factor
L	Annual production rate (units/year)
$\dot{m}$	Mass flow rate (kg/s)
N	Rotational speed (krpm)
p	Pressure (Pa)
Pr	Prandtl number
PW	Power (W)
PWe	Electric power output (W)
q_H	Input heat to the MGT (W)
t	Lifetime period (years)
T	Temperature (K)
U	Overall heat transfer coefficient (W/m^{2}K)
υ	Flow velocity (m/s)
V	Voltage (V)

Subscripts

01…06	Station numbers
amb	Ambient properties
c	Compressor/recuperator cold side
dp	Design point variable
h	Recuperator's hot side variables
recp	Recuperator variables
recυ	Receiver variables
ref	Reference value
t	Turbine variables

Abbreviations

DNI	Direct Normal Irradiance (W/m^2)
HSA	High speed Alternator
IDP	Initial Design Point
LCOE	Levelised Cost of Electricity
MGT	Micro Gas Turbine
MINC	Minimum Cost design
NTU	Number of Transfer Units
TET	Turbine Exit Temperature (K)
TIT	Turbine Inlet Temperature (K)

micro gas turbines have the immediate advantage of 100% clean power production. Additionally, the investment and maintenance costs are lower than hybrid systems because of simpler system and no fuel consumption. However; to the best of authors' knowledge, there have been only a few solar micro gas turbine (sMGT) research projects with solar-only configuration which are the pioneering work by NASA on a 10kWe MGT coupled with a parabolic dish system [12], the integration of a 65kWe Capstone MGT to a solar receiver [13], OMSoP [14,15] and SolGATS. The authors participated in the last two projects as the lead for the design and development of the MGT system. A 5kWe pure solar dish-MGT was developed and tested within the EU funded OMSoP system to demonstrate the potential of the dish-MGT technology as an alternative to dish-Stirling systems which have not yet been successfully deployed to the market despite their reasonable efficiencies [16]. Small scale systems with power ratings below 30kWe, could supply electric power demands of the individual domestic and commercial buildings, when grid back up power is available. Such systems have also the potential to be used as modular dish-MGT units for larger power plants.

There are still several technical and practical problems in the development of small MGTs for dish-MGT systems including the complicated rotor dynamics given the variable insolation effects [17], the advanced power electronics to control the hi-frequency motoring-generation [18], hi-speed shaft sealings and bearings and thermal management of the MGT [19]. Nevertheless, apart from the research undertaken to address those challenges, the key point for the deployment of solar powered systems is to achieve competitive cost of electricity which can be sold to the grid or directly used within the installation. This requires optimisation of the system design which allows for an effective trade-off between thermodynamic and economic performance of the system. According to Osborne et al. the dish-Stirling systems can generate electricity with a cost of about 270€/MWh [20] while for the hybrid solar powered dish-MGT systems the electricity cost is expected to be between 124€/MWh to 140€/MWh [21]. However, that cost is still not very attractive compared to the predictable cost of electricity for PV or the combustion-only (fossil fuelled) systems. The former can achieve electricity costs in the region of 55€/MWh to 80€/MWh [22] and for the latter it is between 40€/MWh to 120€/MWh [23].

Several studies have been done on the design optimisation of the solar powered systems with many of them focused on hybrid solar configuration [24–27]. Hybrid solar systems are normally assumed to work at their design point due to the application of auxiliary combustion. As a result, their overall performance of the

system is a direct function of rated power [28,29]. However, performance of the pure solar MGT is affected by the variations of the direct normal irradiance (DNI). Therefore, a reliable off-design performance model should be used to evaluate the overall generated power by the system during a given period of operation. A quick and easy approach is to apply empirical models for the off-design performance as used in Refs. [30,31]. However, considering the variations of DNI, it is difficult to use such relations for pure solar MGT systems with confidence. These approaches are normally limited to specified power ranges and do not include the effects of components performance on the overall power generation by the system. More importantly, the system performance is highly affected by its operation strategy and safety limits, and it is difficult to take such effects into account when a general model is used. The importance of the chosen operation strategy for the overall generated electricity and the corresponding control logics have been already studied [32]. Detailed off-design modelling to evaluate the system performance considering the components design and DNI variations has been performed by Giostri and Macchi [33] and Semprini et al. [34]. Those two studies resulted in more realistic performance evaluation of the system including the annual generated electricity which is the main performance indicator of a solar-only MGT. Despite their valuable work of including details of system design in the performance model, the analysis is limited either to a single pre-determined design (Giostri and Macchi's work) or a choice of four initial design points which have been generated based on the on-design optimisation (the work of Semprini et al.). As such, the off-design performance of the sMGT has not been considered in the optimisation procedure which is one of the purposes of the present work.

This paper introduces a comprehensive method which uses a components-based system model for the calculation of the off-design performance under the effects of realistic operational conditions including variations of DNI and the operation strategy. A genetic algorithm multi-objective optimisation is used to achieve minimum LCOE and investment cost of the system. The challenge of generating the components performance maps at the design stage of the system has been addressed by including a scaling method within the genetic algorithm to generate the maps from existing initial data. This technique, which has been used before in other contexts, has provided the added value for the present work to take realistic working conditions of the dish-MGT system into account for a techno-economic analysis. The developed method has been discussed first and then the results for two separate cases have been presented and discussed. The first case is for a 5kWe solar only MGT based on the prototype developed in OMSoP project. The second case allows for the rated power to change between 5kWe to 30kWe to find an optimal size for the sMGT systems. A number of plans for the further research are proposed at the end.

2. Methodology and system model

The dish-MGT system configuration which is considered in this paper is shown in Fig. 1 and comprises a single shaft recuperated micro gas turbine engine, a parabolic dish concentrator and a solar receiver (RECV). The micro-gas turbine is equipped with a solar receiver instead of the conventional fuel combustor to use the concentrated solar radiation from the solar dish to heat the air to the required turbine inlet temperature (TIT). The generated power from the turbine is used to drive the compressor and the high-speed alternator (HSA).

The methodology of this paper is based on building a dish-MGT system model which can generate components maps and simulate off-design performance of the system for the full range of operation

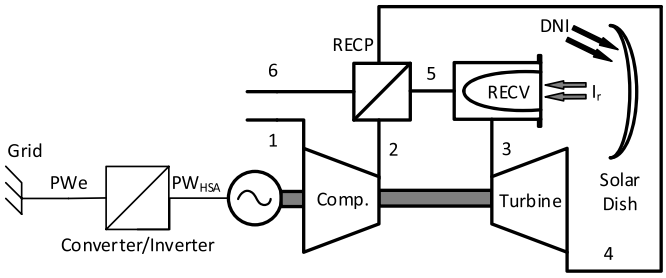

Fig. 1. Schematic of the dish integrated single shaft recuperated sMGT.

only by receiving minimum amount of data of the system design point. The system model also includes a module to evaluate the economic indicators just by receiving the design point data of the system. Those economic and thermodynamic performance indicators include elements of the CAPEX (capital expenses), OPEX (operational expenses), annual generated electricity and LCOE. To obtain an accurate understanding of the potential of solar-only dish-MGT systems for solar power generation, a trade-off between the system costs and performance is required which is achieved through multi-objective optimisation of the system for the mentioned parameters.

The calculation and analysis framework of this paper is depicted in Fig. 2 and is comprised of two main sections, OPTIMISER which uses a genetic algorithm to generate or modify the values of the decision variables [χ] and MODEL which calculates the objective functions Φ[χ] for any set of the given decision variables. An optimisation module from MATLAB has been used for the OPTIMISER which is coupled with the performance simulation code in MODEL. The two sections communicate in MATLAB environment. The objective functions Φ[χ] are the annual generated electricity, E_{an} and specific cost of investment, c_{inv} and the decision variables [χ] are the main system design parameters which affect the thermo-economic performance and consequently, the objective function values.

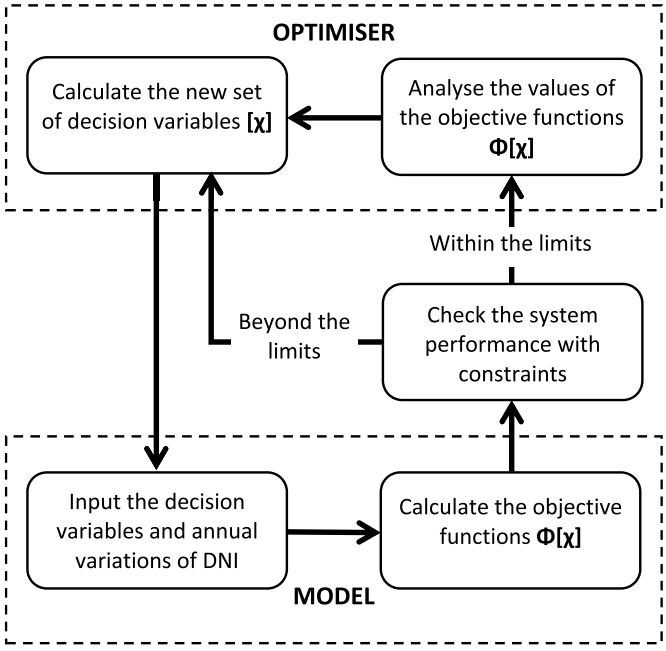

Fig. 2. Diagram of the optimisation framework.

2.1. Multi-objective optimisation

Two objective functions are considered, the investment cost of the system and the amount of the annual generated electricity. To avoid the uncertainties associated with weighted functions approach which converts the multiple objectives to a single function, the concept of Pareto optimality has been used. As shown in Fig. 3, for two objectives of the optimisation problem here, there is a Pareto frontier which represents the optimised systems designs. Any other feasible design will have at least one of the objectives worse than the Pareto frontier.

2.2. Performance simulation

Performance simulation of the dish-MGT system at design and off-design conditions is performed by a computational model which has been specifically developed for such systems [35]. Fig. 4 shows a schematic of the general structure of the model. The core includes the thermodynamic model that requires the components performance maps or sub-models. DNI, ambient temperature, pressure and relative humidity are supplied to the model through the climate condition section. System constraints define the safe operational limits of the system such as the maximum allowable temperatures for the recuperator and solar receiver. These are typically related to design specifications of these components. The boundary conditions determine the electrical load applied on HSA by the control system to set the operation strategy of the micro gas turbine as explained later. The design data section provides the chosen design point data including TIT, compressor pressure ratio, standard ambient conditions and DNI for the design point. The design point performance is calculated by the core module for a set of given design data. This provides enough data for the map generation section to provide the new performance maps during the optimisation process. For each component, the new performance map is generated by appropriate scaling of an existing map. The scaling is done by matching the characteristics of the design point at the initial performance map to the new design point. Further details on the scaling method can be found in Ref. [36].

2.3. Thermodynamic model

The thermodynamic model in the core (Fig. 4) is components based zero-dimensional model which uses components

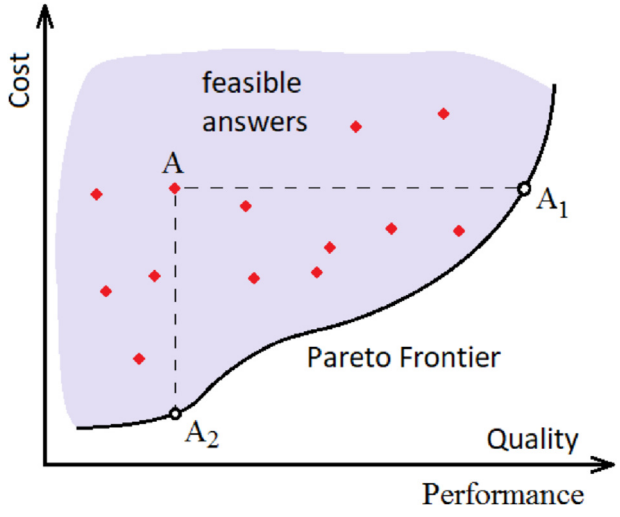

Fig. 3. Pareto optimality.

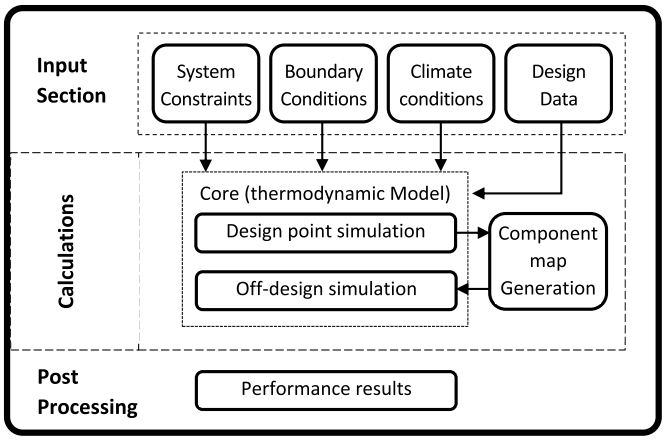

Fig. 4. General structure of the computational model.

performance maps and hence does not require geometrical design data. As such, the model requires a minimum level of data for generating new performance maps for any chosen design point. This is beneficial for the developed method here which requires to run the above sequence for thousands of times when genetic algorithm is used for the optimisation of the system. The performance maps of the components are represented by a number of often non-dimensional parameters which are briefly introduced here followed by the governing equations used in the thermodynamic model.

- *Compressor and turbine*

The characteristics of the compressor and turbine are represented by their adiabatic efficiency η, and reduced mass flow rate $\left(\frac{\dot{m}\sqrt{T_{01}}}{p_{01}}\right)$, as functions $(f_\eta, f_{\dot{m}})$ of the pressure ratio (π) and corrected speed $\left(\frac{N}{\sqrt{T_{01}}}\right)$. [37]

$$\eta = f_\eta\left\{\pi, \left(\frac{N}{\sqrt{T_{01}}}\right)\right\} \quad (1)$$

$$\left(\frac{\dot{m}\sqrt{T_{01}}}{p_{01}}\right) = f_{\dot{m}}\left\{\pi, \left(\frac{N}{\sqrt{T_{01}}}\right)\right\} \quad (2)$$

For any given inlet total pressure (p_{01}), total temperature (T_{01}), rotational speed (N) and pressure ratio (π), the efficiency and mass flow rate can be calculated from the characteristic maps. To facilitate extracting compressor and turbine information from these maps, the auxiliary coordinate, β which was introduced in Refs. [38,39] is used here. For any particular speed, it will be difficult to distinguish between the points close to the surge or chocking limits because there can be more than one point for any given pressure ratio (near surge) or mass flow rate (near chocking). With β lines, only one point can be corresponded to any given speed and β. Besides, the upper and lower limits of β values for all speed lines will be the same. This is not achievable if mass flow rate or pressure ratio are used to represent the map along with speed. Using this parameter, the compressor and turbine maps can be represented by equations (3)–(5).

$$\pi = f_\pi\left\{\beta, \left(\frac{N}{\sqrt{T_{01}}}\right)\right\} \quad (3)$$

$$\left(\frac{\dot{m}\sqrt{T_{01}}}{p_{01}}\right)=f_{\dot{m}}\left\{\beta,\ \left(\frac{N}{\sqrt{T_{01}}}\right)\right\} \quad 4$$

$$\eta=f_{\eta}\left\{\beta,\left(\frac{N}{\sqrt{T_{01}}}\right)\right\} \quad 5$$

Once the design point specifications are fixed, the performance maps can be generated by the scaling of the actual performance maps from existing compressors and turbines which are close to the required turbine and compressor, particularly in terms of their rated power and speed.

A reference point on the performance map is chosen which must be matched with the specifications of the fixed design point. This is done by multiplying the scaling factors to the original map. The scaling factors are calculated based on the fact that they should convert the mass flow rate $[(\dot{m}\sqrt{T}/p)_{ref}]$, pressure ratio (π_{ref}) and efficiency (η_{ref}) of the reference point to the fixed design point specifications $[(\dot{m}\sqrt{T}/p)_{dp},\ \pi_{dp},\ \eta_{dp}]$ as shown by equations (6)–(8) [40].

$$f_{mass}=\frac{\left(\dot{m}\sqrt{T}/p\right)_{dp}}{\left(\dot{m}\sqrt{T}/p\right)_{ref}} \quad 6$$

$$f_{eff}=\frac{\eta_{dp}}{\eta_{ref}} \quad 7$$

$$f_{\pi}=\frac{\pi_{dp}-1}{\pi_{ref}-1} \quad 8$$

- Recuperator

The recuperator model represents the effectiveness (ε) and pressure losses $\left(\frac{dp}{p}\right)$ across the hot and cold streams against the mass flow rate $(\dot{m})$. The relation between these parameters is determined by the design of the recuperator. The methodology in this paper doesn't use detailed design of components to avoid too many parameters being involved in the system model. Ideally, the model should only use the thermodynamic properties at the inlet and outlet points of the recuperator system. As such, a detailed design of the recuperator should not be included because it will require several assumptions for the geometry of the recuperator. Alternatively, a scaling method is used to generate recuperator performance maps for any given design point. The scaling is based upon the existing performance maps of a recuperator and scaling rules to match the existing map to the new design point of interest. As a result, no geometric data is needed for the map generation, although it will be possible to estimate the design based on the scaling rules and the geometric design of the existing recuperator.

The chosen recuperator is a crossflow plate and fin type. This is a compact type of recuperator and has been used for aerospace and industrial applications for several years [41]. The method for scaling the performance maps of the recuperator is based on the $\varepsilon-NTU$ approach which uses the effectiveness, ε, overall heat transfer factor, UA, fluid properties and the mass flow rate. It is preferred over the other methods such as LMTD because it uses ε and mass flow rate which are the two main recuperator parameters when a new system design point is decided. For a cross flow heat exchanger, the number of transfer units, NTU is calculated by equation (9) when ε and the ratio of the flow heat capacity values, C_r are known [42].

$$\varepsilon=\frac{1-e^{-NTU(1-C_r)}}{1-C_re^{-NTU(1-C_r)}} \quad 9$$

$$C_r=\frac{C_{max}}{C_{min}} \quad 10$$

The heat capacity values, C_{min}, C_{max} are products of mass flow rate and heat capacity, $(\dot{m}c_p)$ for cold and hot flows. Utriainen and Sunden have suggested a method which is used here for the overall design of the recuperator and estimation of its off-design performance [43]. Given that the design point data; the effectiveness, allowable pressure drop across each side and the mass flow rate are known, a Reynolds number is assumed for the flow inside the channels of either side of the recuperator. Therefore, the J factor from Colburn analogy and the fanning friction factor, f_F can be estimated for that Reynolds number and the presumed geometry. Fig. 5 shows an example chart for the variation of these factors with Re.

Thus, the heat transfer coefficient, h for each side (hot/cold) is calculated from equation (11) where G is the volumetric flow rate, c_p is the specific heat and Pr is the gas Prandtl number [42].

$$h=\frac{JGc_p}{Pr^{2/3}} \quad 11$$

$$UA=\left(\frac{1}{\eta_ch_cA_c}+\frac{\delta_w}{k_wA_w}+\frac{1}{\eta_hh_hA_h}\right)^{-1} \quad 12$$

Equation (12) will be used to calculate the overall heat transfer coefficient where the indices ″c″, ″h″ and ″w″ denote the properties for the cold side, hot side and interface walls respectively; δ_w is the wall thickness. The iteration is controlled by the overall pressure drop when the estimated friction factor is applied to equation (13) for each side of the recuperator and pressure drop values compared with the chosen values for the design point. If those values didn't match, the Re number must be adjusted and the calculations repeated. In equation (13), f is the flow velocity, L is the characteristic length and L_h is the hydraulic diameter of the flow channel [45].

$$\Delta p_{recp}=\frac{1}{2}\rho f v^2\frac{L}{D_h} \quad 13$$

The off-design performance is calculated using the same set of equations with Reynolds number and heat capacity of the flow

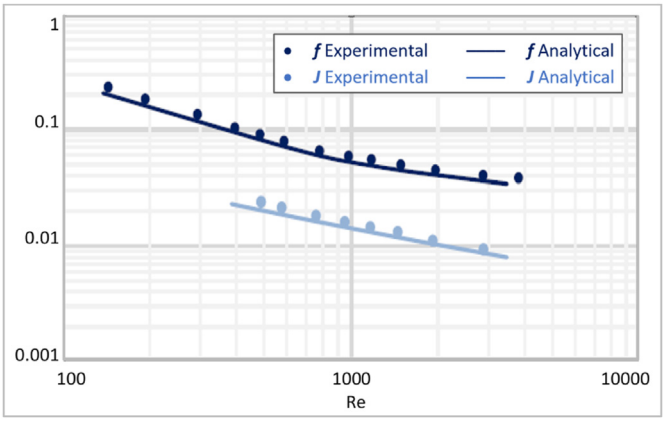

Fig. 5. Variation of Colburn and friction factors with Reynolds number [44].

($\dot{m}c_p$) varying with mass flow rate. The performance charts of the designed recuperator for OMSoP project are shown by Figs. 6 and 7 as an example.

When a new design point is set for the dish-MGT system, the new performance maps will be generated by matching the design point of the existing maps (like Figs. 6 and 7) to the new design point value. The same Reynolds number from the iterative design procedure will be used which results in the same heat transfer coefficient and friction factor. Nevertheless, the overall shape of the recuperator's core will be kept fixed.

- *Dish and receiver*

The performance of the optical system is defined by the optical-to-thermal efficiency (η_{opt}) which is the ratio of heat transferred to the air (q_H) to the solar thermal power received at the dish area (A_{dish}). It can be calculated from the optical-to-thermal efficiency of the dish(η_{dish}), receiver's emissivity (ε_{recv}) and absorptivity (α_{recv}) coefficients, receiver temperature (T_{recv}), concentration ratio (CR_g) and DNI [28].

$$\eta_{opt} = \frac{q_H}{A_{dish} DNI} \tag{14}$$

$$\eta_{opt} = \eta_{dish}\alpha_{recv} - \frac{\varepsilon_{recv}\sigma\left(T_{recv}^4 - T_{sky}^4\right) + U(T_{recv} - T_{amb})}{CR_g\ DNI} \tag{15}$$

T_{sky} is the effective sky temperature which is about 275 K [42].

The second characteristic of the receiver, the pressure loss is a function of its geometry, mass flow rate and temperature. According to Shah and Sekulic [46], the pressure loss in a turbulent flow; which is normally the dominant flow in the receiver, is proportional to the mass flow rate, density and viscosity of air to different powers as shown in equation (16).

$$\Delta p_{recv} = 0.023 \frac{\mu^{0.2}}{\rho} \frac{4L}{D_h} \frac{\dot{m}^{1.8}}{A_o^{1.8} D_h^{0.2}} \tag{16}$$

Other parameters in equation (16), the length L, diameter of the flow path D_h, and the wetted area A_o are all geometrical parameters which are fixed for a particular design. The pressure loss Δp_{recv} will be calculated in Pa when all parameters are used in SI units and therefore the multiplier is dimensionless. The solar receiver configuration is assumed to be a pressurised volumetric cavity receiver which was designed for the OMSoP project. The air flow is in direct contact to the outer side of the cavity. The pressure loss data for different mass flow rates and temperatures are shown by coloured points in Fig. 8 [47]. These points are CFD results generated from a three-dimensional model which is validated against experimental results [48]. Each colour shows a set of pressure loss data against mass flow rate for a given receiver temperature and absolute pressure of 3 bar at the inlet. The dashed lines show the fitted curves for the receiver temperatures of 723 K and 873 K.

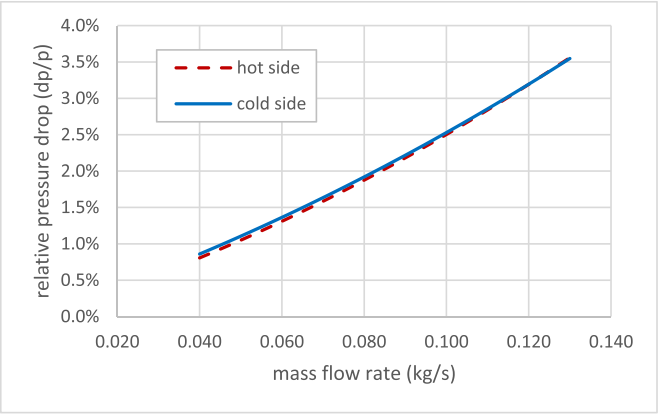

Fig. 7. Pressure losses in the recuperator.

Comparing the fitted curves with equation (16) shows that the multipliers in the fitted formulae represent the effects of the receiver geometry and the properties, density, and viscosity. Those properties are functions of the temperature considering the proportionality of the density with temperature and Sutherland's equation for viscosity of gases, equation (17) [49]. As such, it can be said that the pressure loss relation against the mas flow rate for any given receiver design will be dependent of the air temperature (average temperature for convenience).

$$\mu = 1.5105 \times 10^{-6} \frac{T^{1.5}}{T + 120} \tag{17}$$

Therefore, a relative formula for the calculation of the pressure loss can be derived from the fitted curve for receiver temperature of 723 K as the reference (equation (18)). In equation (18), T_{ref} is the reference temperature (i.e., 723 K) and T_{recv} is the actual average temperature in the receiver in K.

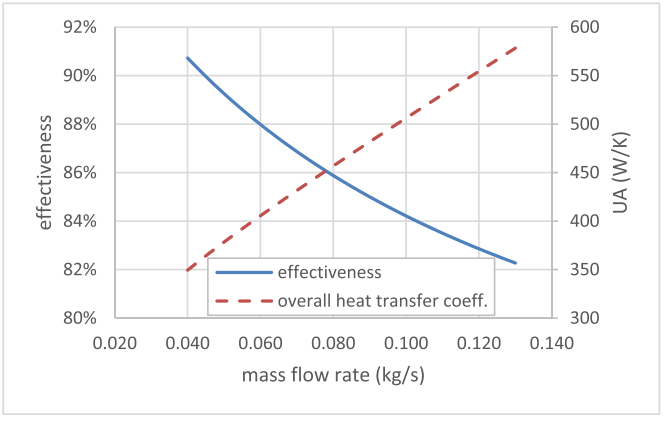

Fig. 6. Thermodynamic characteristics of the recuperator.

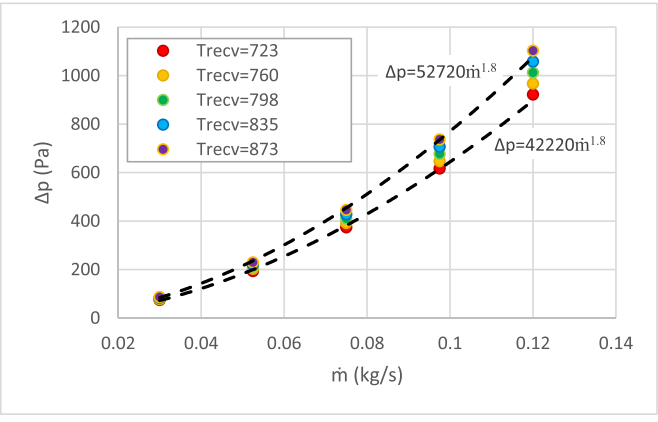

Fig. 8. Correlation for the pressure loss in a cavity receiver.

$$\Delta p_{recv} = 42220\left(\frac{T_{recv}}{723}\right)^{1.3}\left(\frac{723+120}{T_{recv}+120}\right)^{0.2}\dot{m}^{1.8} \quad 18$$

When the inlet pressure to the receiver, p_{recv} is also variable (i.e. during off-design operation), the pressure loss must be corrected considering the absolute reference pressure for the results in Fig. 8, hence:

$$\Delta p_{recv} = 42220\left(\frac{p_{recv}}{3\times10^5}\right)\left(\frac{T_{recv}}{723}\right)^{1.3}\left(\frac{723+120}{T_{recv}+120}\right)^{0.2}\dot{m}^{1.8} \quad 19$$

The maximum error in the estimation of pressure loss caused by using the equation (19) will be less than 1% for the receiver temperature of 873 K which is deemed to be fairly acceptable. For p_{recv} in Pa, T_{recv} in K and mass flow rate in kg/s, the pressure loss will be calculated in Pa.

- *HSA and power electronics*

Fig. 9 shows the architecture of the power generation system. The mechanical power, PW_0 from the micro gas turbine is transferred to the high-speed alternator which converts it to electrical power, PW_1. At this point, the HAS is connected to an Electronic Power Conversion System (EPCS). Such EPCS is composed by a cascade of rectifier (REC) and an active grid connected Inverter (INV). The net electric power PW_e will be fed to the consumer or an electricity grid after voltage losses in the rectifier and inverter. The high-speed alternator will be used as an electricity generator during the period of power generation. It will be used to run the MGT mainly for the start-up of the system when the MGT needs to warm up and reach a certain speed to become self-sustained.

A mathematical model for the high-speed alternator and power electronics (between 0 and 3 in Fig. 9) is required to determine the relation among the main characteristics, rotational speed, output power (PW_e) and electrical efficiency (η_e). The electrical efficiency is defined as the ratio between the electric output power and the mechanical input power.

$$\eta_e = \frac{PW_e}{PW_0} \quad 20$$

The model receives the rotational speed and the input power to the high-speed alternator as the input data. Knowing the electrical characteristics of HSA like its winding resistance, R_{HSA} and inductance, L, the relation between the no-load voltage and generated voltage is calculated by equation (21). The angular velocity is simply calculated from the rotational speed, N. Simultaneous solution of equation (21) and equation (22) which relates the input and output powers of HSA, allows for finding its generated current, I and voltage V_1 [35]. In that equation, k_{HSA} is the power factor of the high-speed alternator and is used for the calculation of the inductive losses.

$$V_0 = V_1 + I\sqrt{R_{HSA}^2 + (L\omega)^2} \quad 21$$

$$PW_0 = PW_1 + 3R_{HSA}I^2 + k_{HSA}N \quad 22$$

The power loss in the rectifier is mainly of the resistive type and can be calculated using the electric current value and its resistance which is almost constant over its operation range. The losses in the inverter are normally 3%–5% and can be assumed as a fixed value. The net output power, PW_e is then calculated from HSA's output power and the mentioned losses in the rectifier and inverter. These calculations can be done for different rotational speeds and produce the performance map of high-speed generator combined with EPCS. Such performance map for OMSoP electrical system is shown in Fig. 10 [35].

- *Governing equations*

The governing equations are provided in form of a set of non-linear equation as represented by equation (23).

$$F(X) = 0 \quad 23$$

For the system configuration shown in Fig. 1, the following equations build the system of equation (23). The numeric indices for temperature, T and pressure p refer to the station points in Fig. 1. In the following equations it is assumed that the flow leakage is negligible.

Conservation of mass:

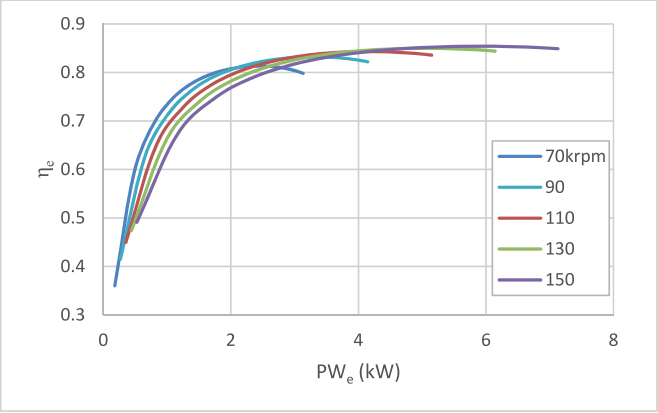

Fig. 10. Overall efficiency of the electrical system.

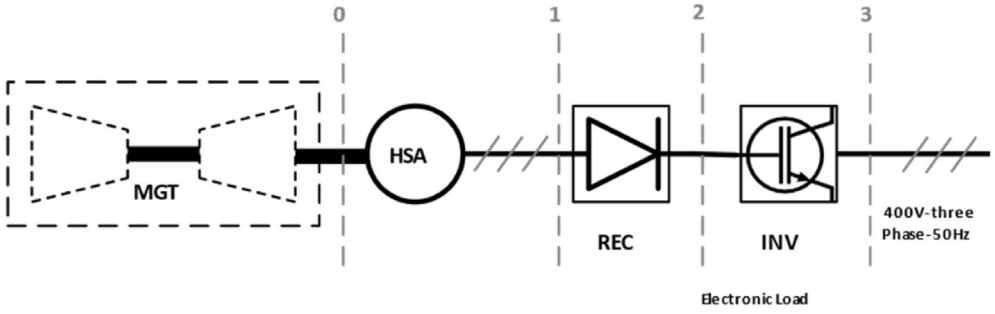

Fig. 9. System arrangement schematic in power generation mode.

$$\dot{m}_c - \dot{m}_t = 0 \tag{24}$$

Conservation of energy:

$$A_{dish}(DNI)\ \eta_{opt} - \dot{m}_t C_p (T_{04} - T_{03}) = 0 \tag{25}$$

Compressor and turbine performances

$$T_{02} - T_{01}\left[1 + \frac{(\pi_c^{(\gamma-1)/\gamma} - 1)}{\eta_c}\right] = 0 \tag{26}$$

$$T_{05} - T_{04}\left[1 - \eta_t\left(1 - \frac{1}{\pi_t^{(\gamma-1)/\gamma}}\right)\right] = 0 \tag{27}$$

$$N_c - N_t = 0 \tag{28}$$

Recuperator performance

$$T_{03} - T_{02} + \varepsilon(T_{05} - T_{02}) = 0 \tag{29}$$

Pressure losses

$$p_{05} - p_{01}\left[1 - \left(\frac{dp}{p}\right)_5\right]^{-1} = 0 \tag{30}$$

$$p_{04} - p_{02}\left[1 - \left(\frac{dp}{p}\right)_2\right]\left[1 - \left(\frac{dp}{p}\right)_4\right] = 0 \tag{31}$$

In the above calculations air is assumed to be an ideal gas and the temperature dependent properties such as the specific heat are calculated using the polynomials given by Ref. [49]. Indices t and c represent turbine and compressor parameters. The relative pressure drops $\left(\frac{dp}{p}\right)_2$ and $\left(\frac{dp}{p}\right)_5$ are for recuperator's cold and hot sides and $\left(\frac{dp}{p}\right)_4$ is for the receiver. The variables for the above system of equations are given by equation (32). There are more parameters used in the above equations which are either given as the input values such as DNI and the ambient pressure and temperature $(p_{01},\ T_{01})$ or can be derived from the components models introduced earlier like pressure losses in the recuperator and the receiver.

$$X = \begin{bmatrix} \beta \\ T_{02} \\ T_{03} \\ T_{04} \\ T_{05} \\ p_{04} \\ \pi_c \\ \left(N/\sqrt{T}\right)_t \end{bmatrix} \tag{32}$$

The parameter, β is an auxiliary coordinate which is used for the compressor and turbine maps to facilitate the locating of the working points on these maps. Any point can be represented by a unique pair of β and speed [39].

Similar to the methodology described by Kurzke, a global iteration approach is used to arrange and solve the equations rather than the traditional nested loop approach (otherwise, called local iteration). This allows to have more flexibility in the program for adding components or changing the cycle arrangement [50].

2.4. Initial design point

Table 1 shows a set of design point parameters for an example dish-MGT system. The upper part of the table includes the parameters which have been assumed for the design point. Those values have been considered based upon thermodynamic cycle analysis and the available technology as suggested in the literature including [51,52] for the turbomachinery, [53] for optical components efficiencies, [41,54,55] for pressure losses and recuperator effectiveness, pressure losses and other component efficiencies. The lower part of Table 1 are the design point parameters which have been calculated using the data provided in the upper part. The nominal system power is set to be 5kWe for this example dish-MGT system which is in accordance with the focus of this paper to investigate small micro gas turbine to be combined with concentrated solar power.

The overall efficiency of the MGT reaches its peak at the design point pressure ratio which is shown in Table 1. However, the efficiency of the system decreases with DNI variations. Therefore, the optimisation of the system is based on the annual performance rather than the design point. Fig. 11 shows the variations of DNI over a sample year in Casaccia where the dish-MGT for OMSoP project is installed.

The performance of the MGT is also affected by the ambient temperature which determines the inlet temperature to the compressor. The variation of the ambient temperature for the chosen area over the course of a year is shown in Fig. 12.

2.5. Operation strategy

It has been already shown that pure solar micro gas turbines can be controlled through an output power regulation to be operated in so-called maximum power production (MPP) strategy [32]. This strategy can be briefly described as a constant TIT operation which uses additional control loops to keep the system within the system constraints which determine the safe operational limits. These limits are:

- Maximum allowable TIT_{max}, which is determined by the receiver and the turbine materials
- Maximum allowable turbine exit temperature TET_{max}, which is determined by recuperator material assuming that the temperature change between turbine exit (i.e TET) and recuperator hot side inlet is negligible.

Table 1
Initial design point data for 5kWe system.

Parameter	value
DNI	800W/m^2
Ambient temperature	288 K
Ambient pressure	1atm
TIT	800 °C
Compressor pressure ratio	3.0
Compressor isentropic efficiency	74%
Turbine isentropic efficiency	80%
Recuperator effectiveness	85%
Concentration ratio	1350
Dish efficiency	90%
Optical-to-thermal efficiency	80%
Electrical efficiency	85%
Dish area	42m^2
Mass flow rate	90(g/s)
Rotational speed	130krpm
Overall efficiency (MGT)	20.7%

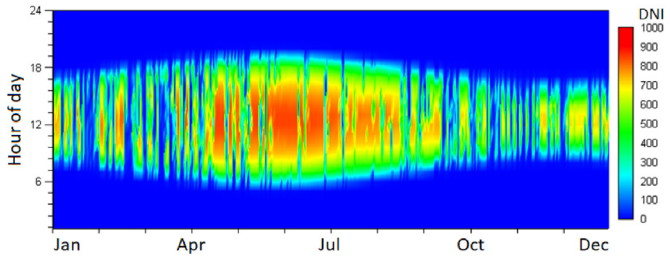

Fig. 11. Sample annual variations of DNI, Casaccia, Italy.

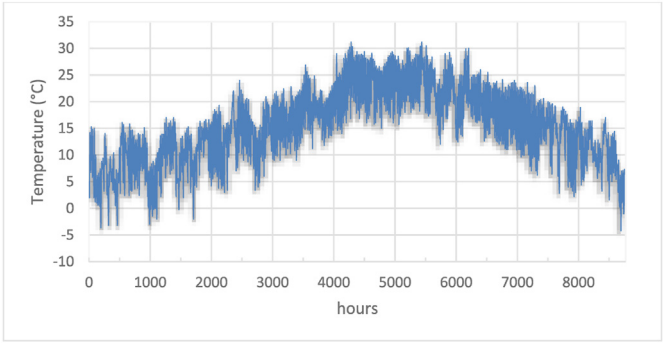

Fig. 12. Sample annual variations of ambient temperature, Casaccia, Italy. Graph generated using the data from EnergyPlus [56].

- Maximum speed N_{max}, which is determined by the rotor-dynamics
- Maximum current in the high-speed alternator I_{max}
- Surge margin which is watched during the off-design calculation

Fig. 13 shows the generated power and overall performance of the system for different DNI values when the MPP operation strategy is applied. The results are presented for a system which is designed based on the design point shown in Table 1. The figure also compares the generated power and MGT efficiency when the correlations provided by Gallup and Kesseli are used [30] when DNI is changing and it shows how the system achieves better performance when the MPP operation strategy is considered.

The annual generated electricity for the system is given by the integration of generated electricity for average DNI value at specified time intervals.

$$E_{an} = \sum (PW_e)_{\Delta t} \Delta t \tag{33}$$

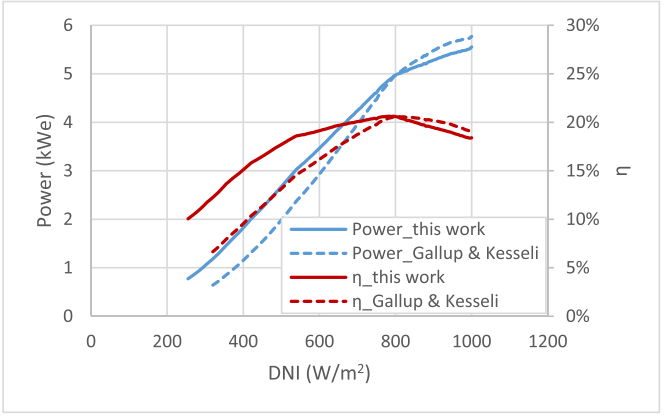

Fig. 13. Comparing system performance with MPP operation strategy with a simpler model.

3. Economic model

The economic model provides cost functions required for the calculation of capital and operational expenses as functions of system design and operation parameters. Most of the existing models are developed based on the architecture and cost data for large gas turbines such as work done in Refs. [57–59]. A modified version of these models for micro gas turbines for 100–500 kW has also been developed in Ref. [60]. In this paper, a model which has been developed as part of the OMSoP project for the dish-MGT systems has been used [61]. The advantage of this model is that it includes the optical components for the concentrated solar power and more importantly, the cost functions for components are developed based upon the data for small-scale micro gas turbines. The general structure of the cost functions is briefly discussed here. The details about the contributing parameters and specific functions for the components are available in Refs. [61,62].

The total cost of investment, C_{inv} consists of the cost of the main components, C_{com} cost of the auxiliary systems, C_{aux} and the installation cost C_{inst}.

$$C_{inv} = C_{com} + C_{aux} + C_{inst} \tag{34}$$

The cost of the whole MGT package including the recuperator and high-speed alternator, $C_{MGT,m}$ is given with the equation (35)–(37). Equation (37) determines the effect of production volume per year, L. The cost of MGT is assumed to be a function of its size which is deemed to be decided by its rated mass flow rate $\dot{m}$. The other parameters that can affect the technology level in MGT package are TIT and recuperator effectiveness. Those parameters determine the values of the parameters $a_{MGT,\dot{m}}$, $b_{MGT,\dot{m}}$ and $c_{MGT,\dot{m}}$.

$$C_{MGT,m} = c_{MGT,m} \cdot f_{MGT} \cdot \dot{m} \tag{35}$$

$$c_{MGT,m} = a_{MGT,\dot{m}} \dot{m}^2 + b_{MGT,\dot{m}} \dot{m} + c_{MGT,\dot{m}} \tag{36}$$

$$f_{MGT} = a_{MGT} L^{b_{MGT}} + c_{MGT} \tag{37}$$

The same set of equations are used for other main components in the economic model except that the mass flow rate $\dot{m}$ will be replaced by the rated thermal power for the receiver and dish area for the parabolic dish. The parameters in the RHS of equation (36) will be different for other components. For the receiver, those parameters depend on TIT whereas for the dish and auxiliary components such as electrical boxes and firefighting they will change with dish area. Finally, the installation cost is divided in civil engineering and construction costs, c_{civil} and the commissioning cost, c_{comm} which are given in form of specific costs per dish area.

$$C_{inst} = A_{dish}(c_{civil} + c_{comm}) \tag{38}$$

3.1. Economic performance indicators

The specific cost of investment for constructing a sMGT plant, c_{inv} (€/kWe) is an important incentive figure for the investors. However, it doesn't include the operational expenses and payback period. As such, the levelised cost of electricity is also considered

Table 2
Parameters used for equation 40.

Parameter	Italy	Spain
i, (%)	2.7	3.88
t, (years)	20	20

which is the minimum sale price for the generated electricity for the lifetime period.

$$LCOE = \frac{\alpha C_{inv} + C_{op} + C_{maint}}{E_{an}} \quad 39$$

C_{op} and C_{maint} are the operation and maintenance costs. α is used for converting the capital costs to an annual equivalent considering the lifetime period t and real interest rate i for the country of installation [63]. Table 2 shows the numerical values for these parameters.

$$\alpha = \frac{i(1+i)^t}{(1+i)^t - 1} \quad 40$$

In conclusion to the economic model, the important design parameters which will affect the capital and operational costs are the size of the dish, TIT and air mass flow rate (i.e. size of the micro gas turbine and recuperator). On the other hand, the expected system life time as well as geographic location affect the LCOE. A favourable solar income as well as the economic figures can reduce the LCOE. More importantly, the economy of scale will have considerable impact on the cost of the system and LCOE. Such effects have been discussed in the next section.

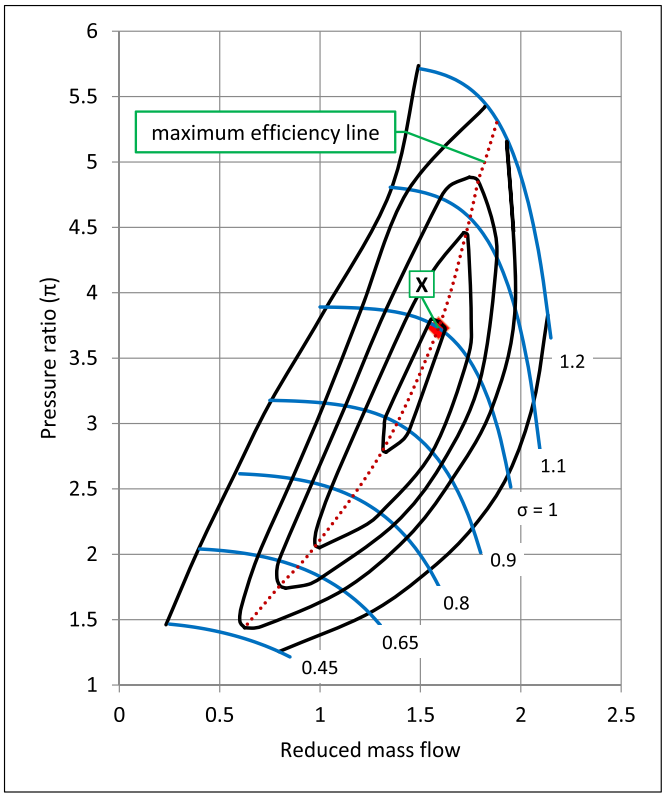

Fig. 14. Representation of parameter σ on the compressor map.

4. Results and discussion

Thermo-economic optimisation problem has been set for two different cases. The first case focuses on a pure dish-MGT system with fixed rated power at 5kWe. Other main design point parameters are set as the decision variable and are allowed to change within their pre-defined boundaries. The objective of the optimisation is to find the numerical values for the system design point which result in an optimal trade-off between thermodynamic performance and capital cost of the sMGT. The second case expands the problem definition of the first case to a wide range of different powers up to 30kWe. The rated power is chosen as one of the decision variables along with the other system design parameters and the maximum value is determined by the upper limit of feasibility for the parabolic dish installations. It should be noted that in both cases, a single dish-MGT system is considered. Hence, the reciprocal shading effect that might be considered in farm arrangement has not been applied in here.

4.1. Problem setup for fixed rated power

Table 3 shows the parameters that are set for the 5kWe solar MGT. The limits for system constraints, TIT_{max} and TET_{max} are defined as the decision variables which allow to define the constraints in parametric form. The efficiencies of the optical components are not included because their effects are monotonic functions and therefore the maximum values with the currently available technology are considered.

The parameter, σ determines the position of the system design point (compressor pressure ratio and mass flow rate) on the compressor map in respect to the maximum efficiency point on the map. Having ($\sigma = 1$), means that the mentioned two points are matching as shown in Fig. 14. In that regard, the parameter σ is essentially representing the ratio of the speeds for the system design point $\left(\frac{N}{\sqrt{T_{01}}}\right)_{dp}$ and the original design point on the chosen compressor map.

The genetic algorithm converges to a Pareto front after 75 generations. Fig. 15 shows the evolution of the generations which ultimately forms a Pareto frontier for a 5kWe to be installed in Casaccia, Italy. The Pareto front represents the optimal designs for the dish-MGT system. Those with higher technology (hence, higher cost) generate more electricity and vice versa. Given that the LCOE is a function of the plant's cost and E_{an}, each optimal design would result in the lowest achievable cost of electricity than any other point in Fig. 15 for the corresponding c_{inv} and E_{an}.

Table 3
Problem setup data.

Decision variable		π_c	σ	ε	η_c	η_t	TIT_{max}	TET_{max}
Decision space	Lower limit	2.5	0.8	0.8	0.7	0.75	750 °C	650 °C
	Upper limit	4.0	1.2	0.9	0.8	0.85	1000 °C	800 °C
System constraints					$TIT < TIT_{max}$ $TET < TET_{max}$ $N_{dp} < 150krpm$			
Objective functions		E_{an}			c_{inv}			

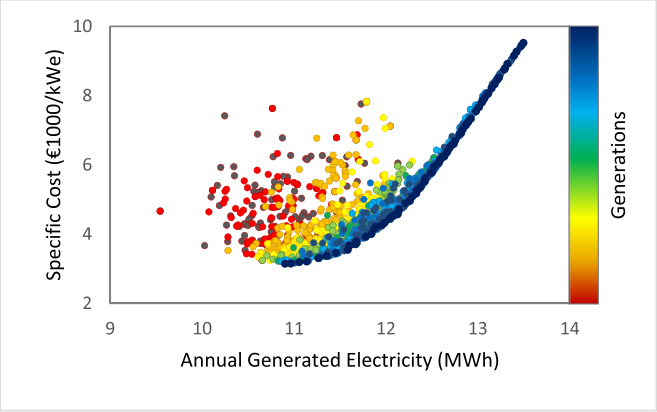

Fig. 15. Evolution of the optimisation results towards Pareto front.

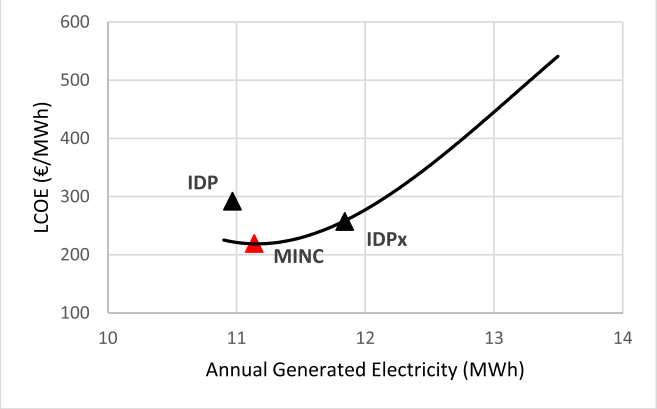

Fig. 16. LCOE for the Pareto solutions.

The LCOE for the optimal designs on Pareto front is shown in Fig. 16 and can be used as a determining parameter to choose for further discussion on the results. The point with minimum value of LCOE is shown in the graph as MINC. Table 4 shows the values of the decision variables (design parameters) of this point. The position of the initial design point (IDP) which was chosen just based on the on-design efficiency can be also seen in the graph. An interesting point on the Pareto front is IDPx which has the same cost of the initial design point but can generate more electricity throughout the year.

Table 5 compares the thermo-economic performances of these points. It can be seen that the optimised design, MINC, requires more than 30% smaller dish area and lower cost with same annual performance as the initial design, IDP.

It is worth noting that the LCOE value is influenced by uncertainties in the input data. The cost estimation for emerging renewable technologies exhibit more variability compared to well-established fossil fuel energy systems. The same argument also applies when comparing the cost models for the mature large gas turbine systems and micro gas turbine that are at the very beginning stages. As such, the solar thermal along with tidal and wave energy systems exhibit significantly more variability in LCOE compared to other renewable and fossil fuel technologies [64].

The breakdown of the capital cost of the system for the initial and optimised design are presented in Fig. 17 which shows how the share of cost of the dish has been reduced because of more efficient system. This is partly because of higher temperature tolerance in the receiver and recuperator which has caused a higher share in the total cost of the system.

Table 4
Specifications of minimum LCOE point on the Pareto front.

π_c	σ	TIT_{max} (°C)	TET_{max} (°C)	ε	η_c	η_t
2.9	1.04	935	727	87%	79%	84%

Table 5
Performance data for the selected points on Pareto front.

Design	E_{an} (MWh)	A_{Dish} (m^2)	c_{inv} (€/kWe)	LCOE (€/MWh)	η_{solar}
MINC	11.06	29.01	3196	219	23.3%
IDP	10.97	42.06	4570	292	15.9%
IDPx	11.84	34.21	4570	257	21.1%

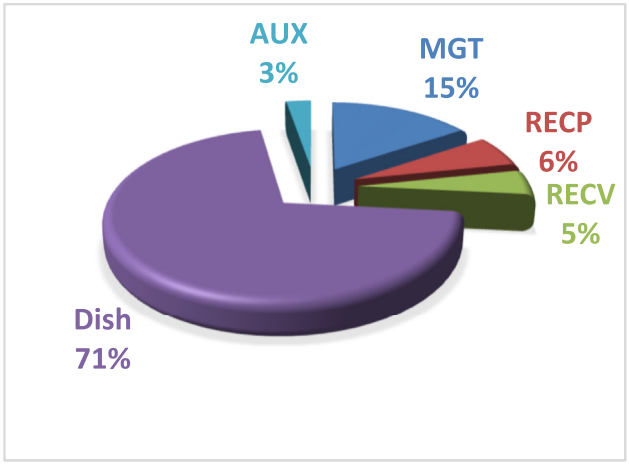

(a)

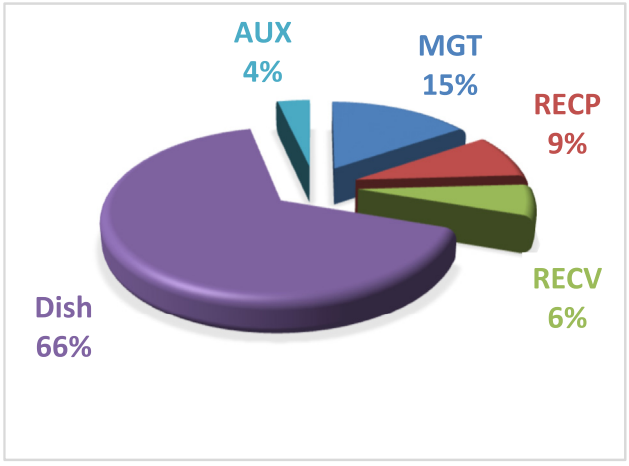

(b)

Fig. 17. Shares of the components in the capital cost of the system a) initial design b) optimised design.

4.2. Effect of annual insolation

To take the effect of annual DNI income, same problem setup as in Table 3 has been done with the environmental data for Seville, Spain. A similar resolution of 10min data has been used for the annual performance calculation. Convergence of the optimisation was achieved after 40 generations as shown in Fig. 18.

With annual DNI income of about 2.25 MWh/m^2 in Seville compared to Casaccia; 1.51 MWh/m^2, the optimised systems have

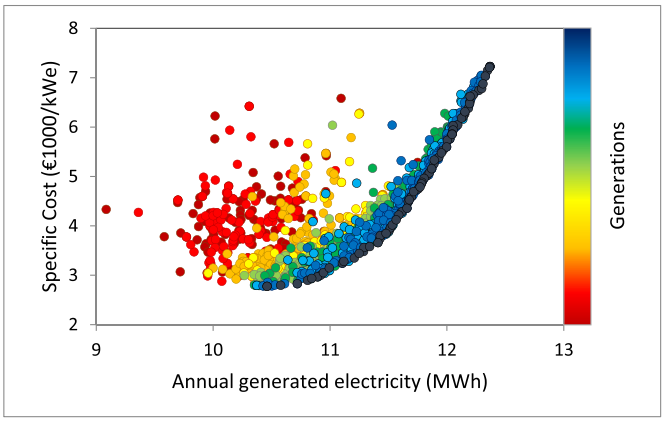

Fig. 18. Evolution of the optimisation results for 5kWe dish-MGT in Seville.

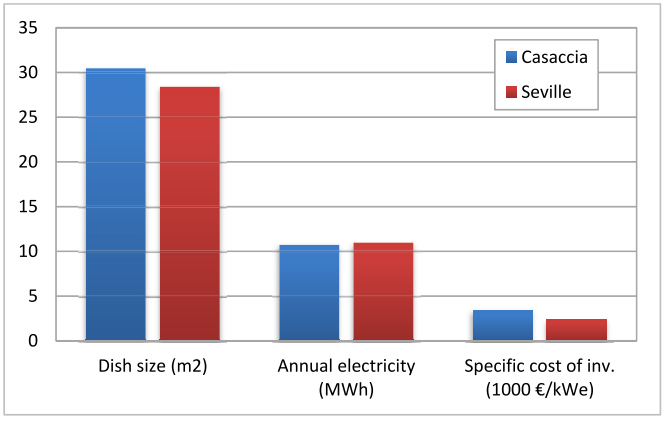

Fig. 19. Comparison of the performance indicators of the optimised designs for Casaccia and Seville.

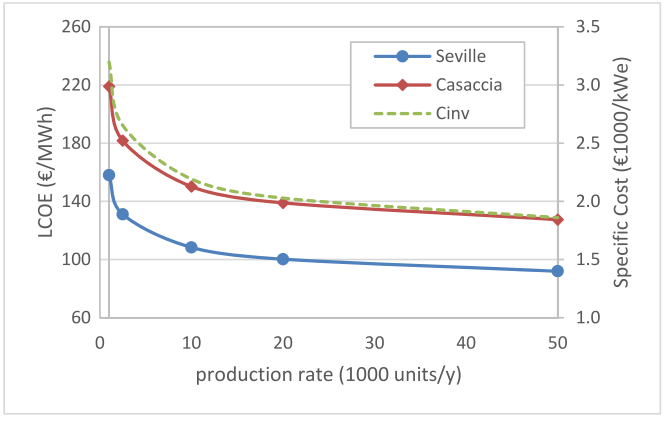

Fig. 20. Cost of electricity for larger production volumes of a 5kWe dish-MGT system.

very close performance as compared in Fig. 19. This is not very unexpected result because the systems have the same rated power. However, the specific cost of the system is clearly lower in Seville than Casaccia as shown in Fig. 19. This has also direct effect on the LCOE which increases from 158€/MWh for Seville to 219€/MWh for Casaccia. Giostri et al. report an LCOE of 175€/MWh for an sMGT powered by an optimised heliostat field and TIT of 950 °C [65].

Compared to the reported cost of electricity for the dish-Stirling systems of about 270€/MWh [20], dish-MGT systems show a promising economic figure. However, this is still far above the cost of electricity from PV systems which is in the range of 55–80€/MWh [22]. One important reason is that PV panels are mass produced. As such, different production volumes have been applied in the calculations for a fair comparison. The cost of the system decreases with the number of units produced per year. The economic model used here considers the economy of the scale for the system components [61]. That has been applied for different production rates and the results are shown in Fig. 20 along with the consequent reduction in the LCOE for larger production volume. For a production rate of 50,000 units per year, LCOE reduces to 92€/MWh in Seville.

4.3. Variable rated power

To investigate the potential of pure solar micro gas turbine systems furthermore, a new optimisation set up is defined in this section to allow for variation of the rated power. As such, systems with different rated power will be included in the decision space of the optimisation problem. From the technical point of view, this results in finding an optimum system size which can generate electricity with lowest cost (i.e., LCOE).

The problem setup is shown in Table 6. The upper limit of the rated power is determined by the maximum dish size as its structure must be strong enough for the wind loads and yet practical to build. The largest practical dishes allow for a rated power of around 25-30kWe. Here, the maximum power is set to be 30kWe. With the variable system size, the cost of the investment is not only a function of system design parameters, but also the system rated power. Therefore, minimisation of C_{inv} causes the optimisation algorithm to tend towards small systems. To address this point, the optimisation task is done with LCOE as the only objective function.

For the above problem setup, the result comes as a single point instead of Pareto line and is represented in Table 7. Calculation is done for Casaccia and it can be observed that the LCOE is much lower compared to the value for optimised 5kWe system. It is also interesting that the optimal design has a power rating of 24kWe which implies that larger systems would have higher cost of electricity. This is because of the parabolic dish which its cost increases after a particular size.

Fig. 21 shows a wider viewpoint on how the thermo-economic performance of the dish-MGT system varies with the rated power. Each point on the LCOE curve, represents the optimised dish-MGT for the corresponding rated power. Although the LCOE reaches a minimum value at 24kWe, it is important to note that its variations at the vicinity of this point is not very substantial. As such, systems

Table 6
Problem setup data.

Decision variable		PWe	π_c	σ	ε	η_c	η_t	TIT_{max}	TET_{max}
Decision space	Lower limit	5kWe	2.5	0.8	0.8	0.7	0.75	750 °C	650 °C
	Upper limit	30kWe	4.0	1.2	0.9	0.8	0.85	1000 °C	800 °C
System constraints						$TIT < TIT_{max}$ $TET < TET_{max}$ $N_{DP} < 150krpm$			
Objective functions		LCOE							

Table 7
Specifications of the optimal design for Casaccia.

PWe (kWe)	LCOE (€/MWh)	Ean (MWh)	Adish (m^2)	Specific cost (€/kWe)
24	170	48.5	113.23	2179.6

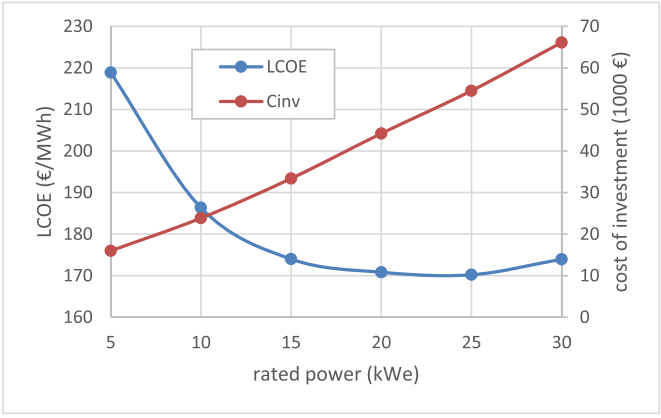

Fig. 21. LCOE and C_{inv} for optimised dish-MGT system with different rated power from 5kWe to 30kWe.

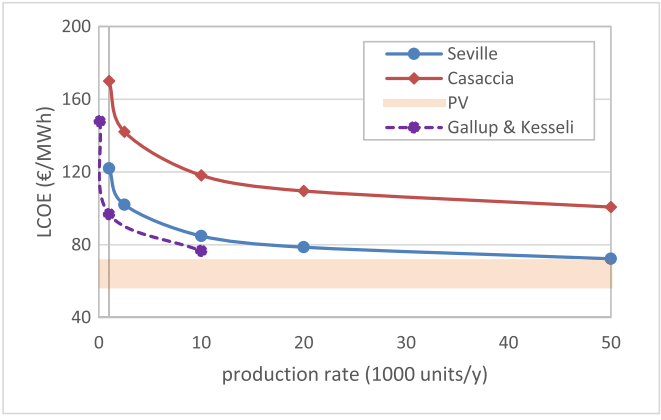

Fig. 22. Variations of LCOE with production volume for the optimised dish-MGT system.

with slightly different rated power can be also considered when a specific power demand is to be matched. Optimisation was also run for Seville, Spain. The optimum rated power of the dish-MGT system was found to be 22.5kWe with the same problem setup as Table 6. At this power, the dish-MGT system can achieve the minimum LCOE of 122€/MWh.

The same scenario similar to Fig. 20 is also done here for Casaccia and Seville and represented in Fig. 22. For each location, the economy of scale has been applied to the optimal size (i.e., 24kWe for Casaccia and 22.5kWe for Seville). The shaded area in Fig. 22 shows the average cost of electricity from PV systems. Considering data for Seville, the LCOE for pure solar dish-MGT systems at an annual production rate of 10,000 units per year reduces to 85€/MWh. This cost figure may sound very promising and probably very optimistic. However, it should be noted that the calculated LCOE is given for relatively large annual generated power. The equivalent rated power in this case will be 225MWe. An LCOE of 122€/MWh is calculated for the annual production rate of 1000 units which is equal to a 22.5MWe solar farm. Fig. 22 also compares the results with the cost of electricity for a similar system in Albuquerque, USA which its average annual DNI is close to that of Seville [30]. Those data are given for volume production of 100, 1000 and 10000 units per year.

5. Conclusion and future work

The thermo-economic optimisation of pure solar dish-MGT systems has been conducted under different scenarios. The objective was to investigate whether such systems, if optimised, can provide electricity at a competitive cost compared to dish-Stirling systems. Furthermore, the optimisations also aimed to establish the position of dish-MGT technology with respect to other solar electric technologies such as hybrid solar MGTs and photovoltaics from an economic point of view. It was found that dish-MGT systems, with rated powers as low as 5kWe, can generate electricity with lower costs than dish-Stirling systems. However, the cost of electricity remains higher than the photovoltaic systems. This difference decreases with the increase in the production volume of the dish-MGT units which could make the technology attractive for potential consumers. It is also found that the annual DNI income and the ambient conditions of the installation site, as well as the local economic figures such as the real interest rate, are significantly influential for the dish-MGT system to be economic. From technical point of view, it was found that there are technical design parameters pertaining to the compressor (pressure ratio, σ) which are not influential on the capital cost, but have considerable effect on the overall system performance and hence LCOE.

It is important to note that in addition to the LCOE, other criteria should also be considered. Although an optimised design results in lower LCOE, it would require a higher level of technology, particularly the MGT, high speed alternator and the receiver. As such, a dish-MGT system may be of more interest for remote or less developed locations despite the higher LCOE.

The proposed method to take the actual off-design performance of the system into account substantially increases the computational time, but adds the value of the optimisation work by taking system design parameters into account as well as the effects of the operation strategy and electricity losses for motoring during low DNI periods. As such, the presented method in this work has the potential to be integrated with more sophisticated components maps generation. This will provide the opportunity to run the system optimisation with more design values particularly the turbine and compressor. This is considered as the next step to the present work.

Credit author statement

Mohsen Ghavami: Conceptualization, Methodology, Formal analysis, software, Writing- Original draft preparation. Jafar Al-Zaili: Methodology, Supervision, Writing- Reviewing and Editing. Abdulanser Sayma: Supervision, Funding acquisition, Writing-Reviewing and Editing.

Declaration of competing interest

The authors declare that they have no known competing financial interests or personal relationships that could have appeared to influence the work reported in this paper.

Acknowledgement

The funding for this research was received through OMSoP project (https://etn.global/research-innovation/projects/omsop/) provided by the European Commission's FP7 programme, grant agreement No 308952, the support of which is gratefully acknowledged.

References

[1] Hewicker C, Hogan M, Morgen A. Power Perspectives 2030: on the road to a decarbonised power sector. European Climate Foundation (ECF); 2011.
[2] Rashid K. Design, economics, and real-time optimization of a solar/natural gas hybrid power plant (Doctoral dissertation). The University of Utah; 2019.
[3] Iaria D, Zhou X, Al-Zaili J, Zhang Q, Xiao G, Sayma AI. Development of a model for performance analysis of a honeycomb thermal energy storage for solar power microturbine applications. Energies 2019;12(20):3968.
[4] Tawalbeh M, Al-Othman A, Kafiah F, Abdelsalam E, Almomani F, Alkasrawi M. Environmental impacts of solar photovoltaic systems: a critical review of recent progress and future outlook. Sci Total Environ 2021;759:143528.
[5] Stamford L, Azapagic A. Environmental impacts of copper-indium-gallium-selenide (CIGS) photovoltaics and the elimination of cadmium through atomic layer deposition. Sci Total Environ 2019;688:1092–101.
[6] H. T. T. L. Şengül, "An environmental impact assessment of quantum dot photovoltaics (QDPV) from raw material acquisition through use," J Clean Prod, vol. 19, no. 1, pp. 21-31, 201.
[7] EU Commission. SOLGATE: solar hybrid gas turbine electric power system. Luxembourg: EU Commission, Directorate-General for Research and Innovation; 2005.
[8] Heller P. SOLHYCO: solar-hybrid power and cogeneration plants. Stuttgart: DLR, Technical Report 019830; 2010.
[9] Quero M, Korzynietz R, Ebert M, Jiménez A, del Río A, Brioso J. Solugas: operation experience of the first solar hybrid gas turbine system at MW scale. Energy Proc 2014;49:1820–30.
[10] Fisher U, Sugarmen C, Ring A, Sinai J. Gas turbine "solarization"-modifications for solar/fuel hybrid operation. J Sol Energy Eng 2004;126(3):872–8.
[11] Sinai J, Sugarmen C, Fisher U. Adaptation and modification of gas turbines for solar energy applications. In: Proceedings of the ASME turbo expo 2005: power for land, sea, and air; 2005. Reno.
[12] English RE. Technology for brayton-cycle space powerplants using solar and nuclear energy. Washington: NASA; 1986.
[13] Dickey B. Test results from a concentrated solar microturbine Brayton cycle integration. In: Proceedings of the ASME turbo expo 2011. Vancouver: Turbine Technical Conference and Exposition; 2011.
[14] EU Commission. Final report summary - OMSOP (optimised microturbine solar power system). London: University of London; 2017. City.
[15] Lanchi M, Montecchi M, Crescenzi T, Mele D, Miliozzi A, Russo V, Mazzei D, Misceo M, Falchetta M, Mancini R. Investigation into the coupling of micro gas turbines with CSP technology: OMSoP project. Energy Proc 2015;69:1317–26.
[16] Mancini T, Heller P, Butler B, Osborn B, Schiel W, Goldberg V, Buck R, Diver R, Andraka C, Moreno J. Dish-Stirling systems: an overview of development and status. J Sol Energy Eng 2003;125(2):135–51.
[17] Arroyo A, McLorn M, Fabian M, Sayma A. Rotor-dynamics of different shaft configurations for a 6 kW micro gas turbine for concentrated solar power. 2016. Seoul.
[18] Al-Zaili J, Sayma AI. Challenges in the development of micro gas turbines for concentrated solar power systems. Brussels: 8th International Gas Turbine Conference; 2016.
[19] Khader MA, Ghavami MA-ZJ, Sayma AI. Heat transfer effect on micro gas turbine performance for solar power applications. Energies 2021;14(20):6745.
[20] Osborn B, Schiel W, Goldberg V, Buck R, Diver R, Andraka C, Moreno J. Dish-Stirling systems: an overview of development and status. J Sol Energy Eng 2003;125(2):135–51.
[21] García-Ferrero J, Heras I, Santos MJ, Pilar Merchán R, Medina A, González A, Calvo HA. Thermodynamic and cost analysis of a solar dish power plant in Spain hybridized with a micro-gas turbine. Energies 2020;13(19):5178.
[22] Ren PS. Renewables 2015 global status report. Paris: REN21 Secretariat; 2015.
[23] Ilas A, Ralon P, Rodriguez A, Taylor M. Renewable power generation costs in 2017. Abu Dhabi: International Renewable Energy Agency (IRENA); 2018.
[24] Schwarzbözl P, Buck R, Sugarmen C, Ring A, Crespo MJM, Altwegg P, Enrile J. Solar gas turbine systems: design, cost and perspectives. Sol Energy 2006;80(10):1231–40.
[25] Spelling J, Laumert B, Fransson T. A comparative thermoeconomic study of hybrid solar gas-turbine power plants. J Eng Gas Turbines Power 2004;136(1):1801–10.
[26] Ssebabi B, Dinter F, Van der Spuy J, Schatz M. Predicting the performance of a micro gas turbine under solar-hybrid operation. Energy 2019;177:121–35.
[27] Aichmayer L, Spelling J, Laumert B. Thermoeconomic analysis of a solar dish micro gas-turbine combined-cycle power plant. Energy Proc 2015;69:1089–99.
[28] Spelling J. Hybrid solar gas-turbine power plants: a thermoeconomic analysis, PhD dissertation. Stockholm: Royal Institute of Technology (KTH); 2013.
[29] Nelson J, Johnson NG, Doron P, Stechel EB. Thermodynamic modeling of solarized microturbine for combined heat and power applications. Appl Energy 2018;212:592–606.
[30] Gallup D, Kesseli J. A solarized brayton engine based on turbo-charger technology and the DLR receiver. In: International energy conversion engineering conference; 1994. Monterey, CA.
[31] Spelling J, Favrat D, Martin A, Augsburger G. Thermoeconomic optimization of a combined-cycle solar tower power plant. Energy 2012;41(1):113–20.
[32] Ghavami M, Alzaili J, Sayma A. A comparative study of the control strategy for pure concentrated solar power micro gas turbines. Charlotte; 2017.
[33] Giostri A, Macchi E. An advanced solution to boost sun-to-electricity efficiency of parabolic dish. Sol Energy 2016;139:337–54.
[34] Semprini S, Sánchez D, De Pascale A. Performance analysis of a micro gas turbine and solar dish integrated system under different solar-only and hybrid operating conditions. Sol Energy 2016;132:279–93.
[35] Ghavami M. Cycle analysis and optimisation of micro gas turbines for concentrated solar power, PhD thesis. London: University of London; 2017. City.
[36] Kurzke J. GasTurb 11: design and off-design performance of gas turbines. 2007. Aachen.
[37] Dixon SL, Hall C. Fluid mechanics and thermodynamics of turbomachinery. sixth ed. Oxford: Butterworth-Heinemann; 2010.
[38] Mirandola A, Macor A. Full load and part load operation of gas turbine-steam turbine combined plant. In: ISEC; 1986. p. 8–15.
[39] Kurzke J. How to get component maps for aircraft gas turbine performance calculations. In: Proceedings of the ASME 1996 international gas turbine and aeroengine congress and exhibition; 1996. Birmingham.
[40] Kurzke J, Halliwell I. Propulsion and power: an exploration of gas turbine performance modeling. Springer; 2018.
[41] McDonald CF. Recuperator considerations for future higher efficiency microturbines. Appl Therm Eng 2003;23(12):1463–87.
[42] Bergman TL, Incropera FP. Introduction to heat transfer. sixth ed. New York: John Wiley & Sons; 2011.
[43] Utriainen E, Sunden B. Evaluation of the cross corrugated and some other candidate heat transfer surfaces for microturbine recuperators. J Eng Gas Turbines Power 2002;124(3):550–60.
[44] D. Iaria, J. Al Zaili and A. Sayma, "Reducing levelised cost of energy and environmental impact of a hybrid micorturbine-based concentrated solar power plant," in Global power and propulsion forum, GPPS-2017-61, Shanghai , 2107.
[45] Gerhart AL, Hochstein JI, Gerhart PM. Munson, Young and Okiishi's fundamentals of fluid mechanics. John Wiley & Sons; 2020.
[46] Shah R, Sekulic D. Fundamentals of heat exchanger design. first ed. New Jersey: John Wiley & Sons; 2003.
[47] Aichmayer L. Solar receiver development for gas-turbine based solar dish systems, PhD dissertation. Stockholm: KTH Royal Institute of Technology; 2018.
[48] Aichmayer L, Garrido J, Wang W, Laumert B. Experimental evaluation of a novel solar receiver for a micro gas-turbine based solar dish system in the KTH high-flux solar simulator. Energy 2018;159:184–95.
[49] Walsh P, Fletcher P. Gas turbine performance. second ed. UK: Blackwell Science; 2004. 2nd ed., Oxford, UK: Blackwell Science, 2004.
[50] NATO R. Performance prediction and simulation of gas turbine engine operation for aircraft, marine, vehicular, and power generation. 2007. NATO RTO Applied Vehicle Technology Panel (AVT).
[51] Rodgers C. Low cost microturbines via the turbocharger route. In: Proceedings of the ASME turbo expo 2011. Vancouver: Turbine Technical Conference and Exposition; 2011.
[52] Lee JJ, Yoon JE, Kim TSSJL. Performance test and component characteristics evaluation of a micro gas turbine. J Mech Sci Technol 2007;21(1):141–52.
[53] Wu S-Y, Xiao L, Cao Y, Li Y-R. A parabolic dish/AMTEC solar thermal power system and its performance evaluation. Appl Energy 2010;87(2):452–62.
[54] Vick M, Heyes A, Pullen K. Design overview of a three kilowatt recuperated ceramic turboshaft engine. J Eng Gas Turbines Power 2010;132(9):2301–9.
[55] Visser W, Shakariyants S, Oostveen M. Development of a 3 kW microturbine for CHP applications. J Eng Gas Turbines Power 2011;133(4):2301–8.
[56] NREL, "EnergyPlus weather Data Official site," US Department of Energy's (DOE) Building Technologies Office, [Online]. Available: https://energyplus.net/weather. [Accessed 1 6 2018].
[57] El-Sayed Y, Tribus M. Strategic use of thermoeconomics for system improvement. In: Gaggioli RA, Comstock MJ, editors. Efficiency and costing, second law analysis of processes, vol. 235. American Chemical Society; 1983. p. 215–38.
[58] Frangopoulos C, von Spakovsky M. A global environomic approach for energy systems analysis and optimization (Part I). In: Energy systems and ecology: proceedings of the international conference ENSEC'93; 1993. Cracow.
[59] Pelster S. Environomic modeling and optimization of advanced combined cycle power plants, PhD thesis. Lausanne, Lausanne: Ecole Polytechnique Fédérale; 1998.
[60] Galanti L, Massardo A. Micro gas turbine thermodynamic and economic analysis up to 500kWe size. Appl Energy 2011;88(12):4795–802.
[61] Sánchez D. D3.1 Report on system cost analysis, OMSoP project. Brussels: European Turbine Network; 2015.
[62] Gavagnin G, Sánchez D, Martínez GS, Rodríguez JM, Muñoz A. Cost analysis of solar thermal power generators based on parabolic dish and micro gas turbine: manufacturing, transportation and installation. Appl Energy 2017;194:108–22.
[63] Madureira NL. Key concepts in energy. first ed. Lisbon: Springer; 2014.
[64] Tran TTD, Smith AD. Incorporating performance-based global sensitivity and uncertainty analysis into LCOE calculations for emerging renewable energy technologies. Appl Energy 2018;216:157–71.
[65] Giostri A, Binotti M, Sterpos C, Lozza G. Small scale solar tower coupled with micro gas turbine. Renew Energy 2020;147(1):570–83.